Nontrivial strength of van der Waals epitaxial interaction in soft perovskites

Yiping Wang, Lei Gao, Yunbo Yang, Yu Xiang, Zhizhong Chen, Yongqi Dong, Hua Zhou, Zhonghou Cai, Gwo-Ching Wang, and Jian Shi

The Non-trivial Strength of van der Waals Epitaxial Interaction in Soft Perovskites

Yiping Wang[1], Lei Gao[2, *], Yunbo Yang[3, Δ], Yu Xiang[3], Zhizhong Chen[1], Yongqi Dong[4], Hua Zhou[4], Zhonghou Cai[4], Gwo-Ching Wang[3], Jian Shi[1, *]

1. Department of Materials Science and Engineering, Rensselaer Polytechnic Institute, Troy, NY, 12180, USA
2. Corrosion and Protection Center, Key Laboratory for Environmental Fracture (MOE), University of Science and Technology Beijing, Beijing 100083, China
3. Department of Physics, Applied Physics, and Astronomy Rensselaer Polytechnic Institute, Troy, NY, 12180, USA
4. X-ray Science Division, Argonne National Laboratory, Lemont, IL 60439

   [*]Correspondence: shij4@rpi.edu, gaolei@ustb.edu.cn
   [Δ]Present address: Hermes Microvision Inc., San Jose, CA, 95131, USA

Abstract

Van der Waals (vdW) bond is traditionally believed to be orders of magnitude lower than the typical chemical bond (i.e., ionic, metallic or covalent) and hence the effects caused by a vdW interface is thought to be trivial. In this study, by investigating the vdW epitaxial growth of mechanically soft perovskite on the vdW substrate, we obtained the solid proofs of strong, non-negligible vdW interaction. The experimental results illustrate the formation of cracks and holes for the relaxation of vdW strain as well as a lattice-constant dependent epitaxial angle evolution and a pronounced band structure change. The first-principle calculations indicate that the contribution of the vdW interaction energy at the epitaxial interface reaches up to more than a quarter of the overall interaction energy far exceeding the traditionally recognized vdW bonding strength. Both the experimental and theoretical work show that given the appropriate material system, the vdW interaction could be strong enough to significantly manipulate material properties.

The van der Waals (vdW) interaction is a dipole-dipole force(*1*) that is traditionally considered much weaker than a chemical bond which involves a permanent charge transfer/sharing process. Consequently the vdW bonding strength is normally thought as trivial and can be easily disturbed or altered. By taking advantage of that, mechanical exfoliation was first applied to obtain the atomically thin two dimensional graphene from graphite(*2, 3*), together with a whole family of two dimensional materials including h-BN(*4*), transition metal dichalcogenides(*5, 6*), etc. As a step forward, heteroepitaxy is found to exist between two different vdW bonded materials and hence comes the vdW epitaxial growth(*7, 8*). Different from the traditional chemical epitaxy, vdW epitaxy lifts the restriction of rigid lattice match and even lattice symmetry thanks to the weaker interfacial interaction(*7, 9, 10*). VdW epitaxially grown thin films are usually believed to be in a freestanding nature with few defects that can lead to a high mobility and good properties(*10, 11*). Over the years, various materials have been proven to grow epitaxially on a single mica substrate by vdW epitaxy[8], which includes both naturally layered materials (transition metal dichalcogenides, metal halides, etc.) and non-layered materials (halide perovskite, metal oxides, group II-VI materials, etc). Like a double edge sword however, vdW epitaxy largely broadens the material selection but at the same time is generally believed to be unable to manipulate the overlayer property via substrate effect. However, if indeed strain engineering also exists in the vdW epitaxy, one of the major benefits would then be the capability to strain materials that are hard to obtain via conventional epitaxy, i.e., materials whose suitable substrate are yet to be found.

Despite the above commonly accepted understandings of vdW interaction, there are more and more observations that indicate otherwise as the research on two-dimensional materials deepens. For example, ultraflat graphene is and can only be obtained when muscouvite mica, a layered substrate, is supported underneath(*12*). The experimental observation as well as subsequent theoretical work(*13*) both indicate a strong interaction that can be vdW in nature. At the same time, a strong interlayer electron-phonon interaction between h-BN and WSe_2 was observed(*14*), indicating a non-trivial vdW interface. For the epitaxial vdW heterostructure, largely-strained growth of organic thin film on mica substrate has been demonstrated(*15*). Recently for the pure inorganic material system, an incommensurate-commensurate transition was observed for h-BN and graphene that resulted in a large vdW strain(*16*). Previously we have also studied the possible vdW strain engineering on PbI_2(*17*). Even for a quasi vdW epitaxial growth, e.g. only one of the film/substrate is a layered material, it is found that the choice of substrate can result in a significant strain of an presumably strain-free two dimensional material(*18*).

With the discrepancy between the assumptions and observation in vdW interaction, there are, of course, intriguing questions remains to be answered. Since the interlayer vdW interaction is so trivial, why can epitaxy always be formed? When a quasi-vdW epitaxy is formed, what is the nature of the interface interaction? Is there a case when vdW interaction could be strong enough so that the conventional strain engineering occurred in chemical epitaxy can be repeated? Can the vdW interaction be more pronounced if the growth material is mechanically soft in nature and at the same time contains heavy elements since the vdW interaction scales with atomic weight? In this report, we attempt to address these questions by studying the vdW epitaxial growth of $CH_3NH_3(MA)/CsPbX_3$, an emerging semiconducting material family with Young's modulus ranging from 14 to 19 GPa(*19-21*), on mica substrate.

From our previous experience with the halide perovskite(*9, 22*), single crystalline and epitaxial flakes were grown. Thanks to the soft nature of the halide perovskite material(*23*), we found solid evidence both from morphology, structural and optical characterizations that indicate a very strong, non-negligible vdW interaction existing between mica and halide perovskite and the possible existence of significant vdW strain. By performing the density functional theory (DFT) calculations, we studied the nature of bonding at the halide perovskite/mica interface and revealed the indispensable role of vdW interaction. Our study shows that by the proper selection of the material systems, the strength of vdW epitaxial interaction can be fully unleashed to achieve the promising vdW epitaxy-based strain engineering.

Epitaxial halide perovskite has been grown on mica substrate via Chemical Vapor Deposition (CVD) with controlled parameters that can influence the flake size and thickness. Additional information concerning the details of the growth setup can be found in the materials growth and characterization in the Supplementary Information (SI) (*24*). Fig. 1(a) shows an optical image of the large scale epitaxial growth of MAPbBr$_3$ flakes about ~10 μm in lateral size on mica substrate. It can be easily observed that all the flakes show a square/rectangular morphology that corresponds to the Wulff construction of the {100} lowest surface energy facets. Meanwhile, the flakes are well aligned towards one single direction that indicates a well-constructed epitaxial relation with the substrate. Moreover, the as-grown flakes show a similar weak color contrast under optical microscope, indicating a uniform and relative small thickness. A closer examination of the morphology and thickness profile of the same flakes was performed by Atomic Force Microscope (AFM), with the resultant image shown in Fig. 1(b). The AFM images shows that the halide perovskite has a smooth surface across the whole flake that is comparable to the atomically flat mica surface. The thickness of the individual flakes ranging from 4.8-16 nm has been labeled. A similar AFM image with a larger scale that contains more flakes can be found in Fig. S1. The thinnest flake we have been able to grow so far is about 6 atomic layers of MAPbBr$_3$. The inset of Fig. 1(b) shows a relatively thicker flake (~31 nm), nonetheless it has the same surface smoothness. A more clearly quantitative illustration of the thickness profile of three individual flakes are shown to the right of Fig. 1(b), with the surface of each flake showing no observable thickness variation.

However, as the flake grows in both lateral size and thickness, a completely different situation was observed, as will be discussed later in Figs.1 (c) to (e). Fig. 1(c) shows a large CsPbBr$_3$ flake with its lateral size exceeding 100 μm and thickness over 100 nm. Surprisingly, well-aligned crack networks parallel to the edges along <100> directions can be easily observed even in the optical microscope. As a step forward, we found for even larger area CsPbBr$_3$ "thin film", not only cracks but also square holes, as displayed in Fig. 1(d). It can be easily seen that for the square holes in Fig. 1(d), still the <100> edge dominates. That the appearance of cracks and holes in thicker and larger flakes and the absence of those in thinner ones, even though both are epitaxial in growth, is of great interest. Holes and cracks are commonly interpreted as signatures of strain relaxation once the film thickness exceeds a critical limit in the conventional chemical epitaxial growth of thin film(*25, 26*). The appearance of those, especially in thicker flakes, indicates that for vdW epitaxy, the interaction at the flake interface is comparably strong and more importantly, the thinner, crack

and hole-free flakes may be highly-strained due to the soft nature of halide perovskite. To investigate the nature of the morphology of the holes, AFM characterization was further conducted and shown in Fig. 1(e). Consistent with the observation made in optical images, AFM shows holes on single flakes with sharp <100> edges. Moreover, we also observe at the vicinity of the square hole very clear layer-by-layer terraces with the step height equal to one atomic layer of MAPbBr$_3$, as shown by the height profile to the right of Fig. 1(e). A magnified view of the layer-by-layer terrace can be found in Fig. S2. The presence of terraces, i.e., the Stranski-Krastanow (SK) growth, is also another typical sign of strain relaxation, although less drastic, compared to the formation of cracks and holes(27, 28). In addition to that, we also observed trench networks 45° to the hole edges (i.e., along <110> directions). The trenches could be another sign of the SK growth mode and the formation of islands to accommodate strain. More AFM image concerning the relative orientation of the hole edges and the 45° steps can be found in Fig. S3.

While the morphologies of the as-grown vdW epitaxial halide perovskite flakes show solid evidences of strong interface interaction, the resultant strain and strain relaxation is likely to render a structural reconstruction of halide perovskite compared with the bulk crystal. To investigate the structural information of the epitaxial growth, both synchrotron X-ray diffraction (XRD) and Transmission Electron Microscope (TEM) studies were carried out. Figs. 2(a)-(b) shows the result of synchrotron XRD characterization of the MAPbBr$_3$ flake on mica substrate under a reflection mode (i.e., the out-of-plane lattice spacing is measured). Taking advantage of the nano beam, we were able to focus the synchrotron X-ray flux into a ~500 nm spot so that the diffraction information of a single flake can be acquired. Unfortunately, due to the extensive beam damage, only relatively thick flakes can be characterized. Fig. 2(a) shows the rocking curve of MAPbBr$_3$ (002) with a Full-Width-at-Half-Maximum (FWHM) less than 0.05°. This again confirms the high quality single crystallinity of the as-grown flakes. Fig. 2(b) shows the θ-2θ out-of-plane scan with the (006) and (008) reflection of mica substrate and (002) reflection of MAPbBr$_3$ cleared presented. Interestingly in addition to those, one extra reflection (which is labelled as "interface layer" in Fig. 2(b)) is also observed that can be fit to neither the flake nor substrate. The extra spot is very unstable and would disappear soon after a prolonged synchrotron irradiation. With all available knowledge, we hypothesize that the reflection comes from either an interfacial layer that helps better buffering the MAPbBr$_3$ on mica substrate, or more surprisingly, from a highly strained layer of perovskite at the interface that rapidly relaxes after an external perturbation (e.g., high energy synchrotron irradiation). Meanwhile, when the (002) reflection was checked for individual flakes, we still observe a noticeable peak shift, with the thinner one being smaller in the out-of-plane spacing (Fig. S4), indicating possibly some residual compressive out-of-plane strain. Even though we have been unable to characterize the sub-10 nm flakes, by studying the thicker flakes, we are still able to conclude that the flakes are no longer freestanding and strain-free as previously assumed.

To better understand the structural information of the film's in-plane orientation with the substrate, we carried out in-plane TEM electron diffraction analysis of MAPbCl$_3$ and CsPbBr$_3$ flakes on mica. The CsPbBr$_3$ and MAPbCl$_3$ flakes are chosen due to the feasibility of TEM sample preparation and at the same time we can see how the epitaxial relationship would be modified if halide perovskite with different lattice constant are grown. In general, the samples

4

tested have lateral dimension of about micrometers according to the TEM real space image. The thickness cannot be directly measured by the TEM but estimated being < 20 nm based on the growth condition. The resultant TEM diffraction patterns of different crystals are shown in Fig. 2 (c)-(e) where (c) is for $MAPbCl_3$ and (d)-(e) are for $CsPbBr_3$ flakes. All the indices of mica have been accurately labeled based on its monoclinic crystal structure. With the limited in-plane TEM samples we can prepare, surprisingly we found that for $CsPbBr_3$ samples, different flakes indeed show different in-plane lattice constant of 5.77 Å in (d) and 5.86 Å in (e), supporting the argument of epitaxial strain for thinner flakes. More interestingly, we also found that as the lattice constants for different halide perovskite change, their epitaxial relationships with mica substrate also change in a regular pattern. That is, the reciprocal vector offset angle between the perovskite (200) and mica (200) increased from 5.26° to 50.68° as the lattice constant increases from 5.69 Å to 5.86 Å. This progressive angle change is in great resemble to the Novaco-McTague theory(29) where they proposed that when incommensurate epitaxy is formed on a vdW substrate, the incommensurate angle (in our case the angle between perovskite (200) and mica (110)) would gradually change as the lattice constant of the overlayer changes. The angle change itself is believed to be a pathway for strain relaxation. Later experimental results of noble gas adsorption on graphite successfully proved the theory(30) but so far such angle dependent incommensurate epitaxy has yet to be proved in inorganic material systems. Therefore, the angle dependence we found would very likely be the result of vdW strain relaxation and a sound proof of the strong vdW interaction when epitaxy is formed. We believe the observance of the angle dependence is a result of the mechanically soft nature of the halide perovskite and the high mobility of adatoms on a vdW surface. Such angle dependence is again confirmed when we carried out a transmission mode synchrotron diffraction on a group of small epitaxial $CsPbBr_3$ crystals, as shown in the result in Fig. S5. Fig. S5 is a magnified portion of a synchrotron diffraction pattern where the diffraction spot dispersion in radial direction denotes the lattice spacing variation and the dispersion in tangential direction denotes the orientation angle dependence. We can clearly observe that while the diffraction spots for $CsPbBr_3$ has the same "sharpness" as mica in the radical direction, these spots are much more dispersed along tangential direction that is consistent with our angle dependent observation in the TEM characterization. The structural characterizations overall indicate that strain may very likely to exist at least at the early stages of the vdW epitaxial growth of halide perovskite, which will later relaxes either by the formation of cracks/holes or through an incommensurate angle.

Meanwhile, we also believe that if the strong vdW interaction would influence the morphology and structure of halide perovskite, its electronic band structure and optical properties will be altered as well. For that purpose, we conducted photoluminescence (PL) study on $MAPbBr_3$ flakes with different thicknesses and showed the resultant spectra in Fig. 3(a). By observing the color contrast in optical images we can easily identify the relative thickness of the flakes being investigated. Fig. 3(a) shows that with decreasing film thickness, we see a uniform trend of blue shift of PL peaks of $MAPbBr_3$ from about 2.31 eV for solution produced bulk single crystal to 2.44 eV for the thinnest $MAPbBr_3$ flake we have been able to characterize. The insets of Fig. 3(a) are the optical images of the individual samples being tested. The lateral size of all the flakes tested in Fig. 3(a) is around micrometers and their thickness is well beyond the range of quantum confinement. We did not observe any PL

dependence on the lateral size of the flake. The thickness dependent PL blue shift for halide perovskite has been observed and studied for some time(*31-33*), with a conclusive explanation yet to come. However, it should also be noted that our result, together with other experimental work(*33*) on epitaxial growth, produces a much more drastic thickness dependency compared with other non-epitaxial work(*31, 32*). Due to the very recent popularity of halide perovskite, there has been very limited study on the conventional epitaxial growth of the material and we have been demonstrating earlier the epitaxy growth on the NaCl substrate[36]. However, it is found that it is still very challenging to strain the material by NaCl and study the thickness dependent PL in that case. The strain will be completely relaxed for thicker film (so there is no PL shift) and for thinner film, Cl will diffuse into the overgrow layer and mediate the lattice mismatch and the resultant PL will be from the mixed halide perovskite instead of a strained thin film layer. Nonetheless, the finding in this report, to the best of our knowledge, has shown the most significant thickness dependent PL shift. Meanwhile we may also exclude other mechanisms that may result in the PL shift. First, for the reabsorption of self-emitted PL(*34, 35*), such phenomenon can be neglected for thinner flakes and indeed for thicker ones, a shoulder at low energy side starts to show up which can be interpreted as the result of self-absorption. Secondly, we also rule out the Burstein-Moss effect(*36*) since previously an excitation intensity dependent PL of similar flakes by us(*37*) showed no observable peak shift. The intensity dependent PL can also be referenced to rule out the possibility of optical Stark effect, a fluence-dependent energy level splitting phenomenon(*38*). To further verify the peak shift comes from a change in the electronic band structure instead of other dynamics, we performed micro-photoreflectance (PR) study on two flakes, together with their PL results shown in Fig. 3(b). It can be observed that the peak shift in PR spectra is consistent with the PL difference, indicating that excitonic effect is negligible, thus the two flakes indeed differ in the band structure since reflectance is an absorption-related first order effect. With all the discussions above, we have reasons to believe that it is the mica substrate and vdW epitaxy that induce a more drastic PL shift. Besides the aforementioned observations, a comparison between the temperature dependent PL of vdW flakes and bulk single crystals of $MAPbBr_3$ would give rise to another proof of the strong interaction from mica substrate. As shown in Fig. 3(c), upon changing temperature, the peak energy from bulk single crystals changed more drastically than that of vdW flakes. Since for the same kind of material, the electronic band structure is to a large extent determined by lattice parameters, the lattice of bulk single crystal $MAPbBr_3$ changed more drastically compared to vdW flakes. We tentatively attribute this discrepancy to the interaction with mica substrates. Considering the larger thermal expansion coefficient of halide perovskite(*39*) than that of mica(*40*), the thermal expansion of vdW flakes will be reduced by that from mica, thus a larger thermal strain is observed in bulk single crystals. This observation indicates that the vdW interaction might be strong enough to mediate the mismatched thermal strain during various heating/cooling processes.

　　All the experimental results above indicate that the bonding nature between a layered mica substrate and non-layered halide perovskite is much more intriguing than expected and that the qualitative analysis is insufficient to unveil the fundamental physics. With that consideration, first-principles calculations were carried out to understand the interface between mica and $CsPbBr_3$. The inorganic perovskite is chosen due to its structural simplicity

but similar chemical and mechanical properties with its hybrid counterpart. The DFT calculations were carried out in the Vienna *ab initio* Simulation Package (VASP)(*41*). The projector-augmented-wave (PAW) method was utilized to model the core electrons(*42*). The electron exchange and correlation were modeled within the generalized gradient approximation (GGA) using Perdew-Burke-Ernzerhof (PBE)[42]. A non-local optB86b-vdW exchange-correlation functional(*43, 44*) was used to describe the dispersion interaction (vdW forces) approximately, as it has been demonstrated to be among the most accurate vdW functional(*45*). The plane wave basis kinetic energy cut off was set to 400 eV. In the simulation supercell, the mica was selected as the substrate and three layers of $CsPbBr_3$ lattices were covered on the mica surface to simulate the growth interface. The top K atoms layer of mica and the three layers $CsPbBr_3$ lattices were allowed to relax until the forces on all the relaxed atoms were less than 0.05 eV/Å. The rotation angle between the mica and $CsPbBr_3$ was selected as 33.69°, mainly by considering the following reasons: to decrease the macro strain imposed on the $CsPbBr_3$ lattice and reduce the consumption of computational resource.

Fig. 4 (a) is the relaxed mica/$CsPbBr_3$ supercell and we can clearly observe the distortion at the interface of mica/$CsPbBr_3$. Due to the lattice/symmetry mismatch between the mica and $CsPbBr_3$, an incommensurate interface is formed. Fig. 4(b) shows the atomic stacking and charge transfer distribution in the planar view between mica and $CsPbBr_3$, clearly illustrating the distortion at the interface. Fig. 4(c) illustrates the cross section of the blue dashed line noted in Fig. 4(b), where the strong ionic interaction between K layer of mica and PbBr layer of $CsPbBr_3$ could be observed. The existing strain at the mica/$CsPbBr_3$ interface will consequently influence the $CsPbBr_3$ electronic band structure as well as PL spectra, and the effects will attenuate with the $CsPbBr_3$ thickness increasing, which might be closely related with the thickness dependent of blue shift of PL peaks.

The characteristics of the interfacial interactions between the mica and $CsPbBr_3$ is then determined by the contributions of the ionic and vdW interaction through comparing the difference between interaction energies of the nonlocal correlation functional and the one without it(*13*). In the two calculations, we firstly calculated the interfacial characteristics including both the ionic and the nonlocal vdW interactions with the optB86b-vdW functional (shown as the red column in Fig. 4d). Then, utilizing the same atomic structure we calculated the ionic interface properties of the mica/$CsPbBr_3$ with only plain PBE and obtained the blue column in Fig. 4d. Comparing with the two columns, we could distinguish the energy scale of vdW interaction. The obtained results shown in Fig.4(d) indicate that the ionic interactions play the major role at the interface, which is reflected by the effective charge transfer (corresponding to Fig. 4(c)), while the rest contribution of vdW interaction could still reach up to 26.69% (about 20 meV/$Å^2$). This value is already a considerable fraction of chemical bond and goes far beyond the conventional assumption that vdW interaction is orders of magnitude lower than a typical chemical bond. For example, the calculated vdW energy at the interface is about 1/4 of the silicon (111) free surface energy of 76.8 meV/$Å^2$ (*46*), and several times higher than the surface energy of graphene of ~3 meV/$Å^2$ (*47*), a typical value for conventional vdW bonding.

In summary, in this study we made a series of attempts to understand what a "strong" vdW interaction could look like in the soft perovskite system. By the observations of various

possible strain relaxation mechanisms including the formation of cracks/holes, the lattice constant-dependent incommensurate rotational epitaxy and the thickness dependent PL/reflectance, we show that if the material is soft enough, vdW epitaxy can also result in a non-trivial substrate-film interaction. DFT calculations confirmed the vdW interaction in our case can contribute over one-fourth of the interfacial interaction between the soft crystal and the vdW substrate, suggesting a substantial part of the strain-related phenomena could stem from vdW force.

Competing Financial Interests
The authors declare no competing financial interests.

Supporting Information is available online.

Figures and Figure Captions
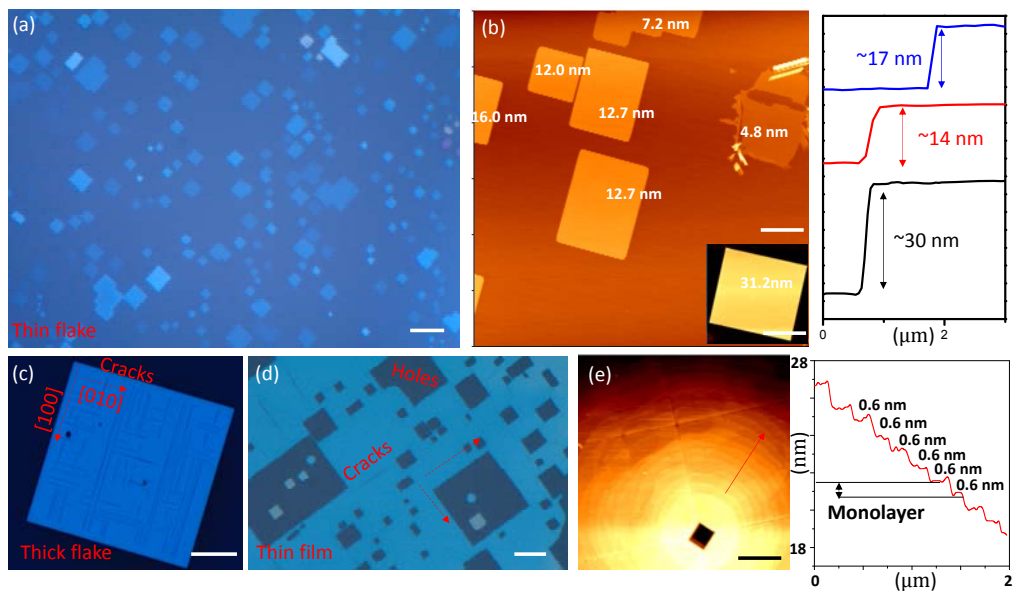
Fig. 1 Morphology characterization of halide perovskite flakes grown on mica substrate.
(a) Optical image of large scale growth of epitaxial MAPbBr$_3$ on mica substrate. The square flakes of halide perovskite are aligned into one direction and the similar color reflects a small thickness variation. (b) AFM characterization of the flakes in (a), the individual flake thickness is labeled. The inset shows another thicker flake also with very smooth surface. The right of (b) shows the thickness profiles of three individual halide perovskite flakes. (c) Optical image of a large, thick CsPbBr$_3$ square flake with perpendicular cracks on the surface. The crystallographic orientations of the crack have been labeled. (d) Optical image of CsPbBr$_3$ thin film with square holes and cracks on the surface. The cracks and holes can be viewed as signs of strain relaxation. (e) AFM characterization of the holes in MAPbBr$_3$ thin film on mica. At the vicinity of the square hole there exist terraces of monolayer thickness (shown by the height profile on the right). Perpendicular lines with 45° to the edge of the square can also be observed, which are hypothesized to be [110] dislocations. (Scale bar: (a) 10 µm; (b) 5 µm; (c) 30 µm; (d) 10 µm; (e) 1 µm)
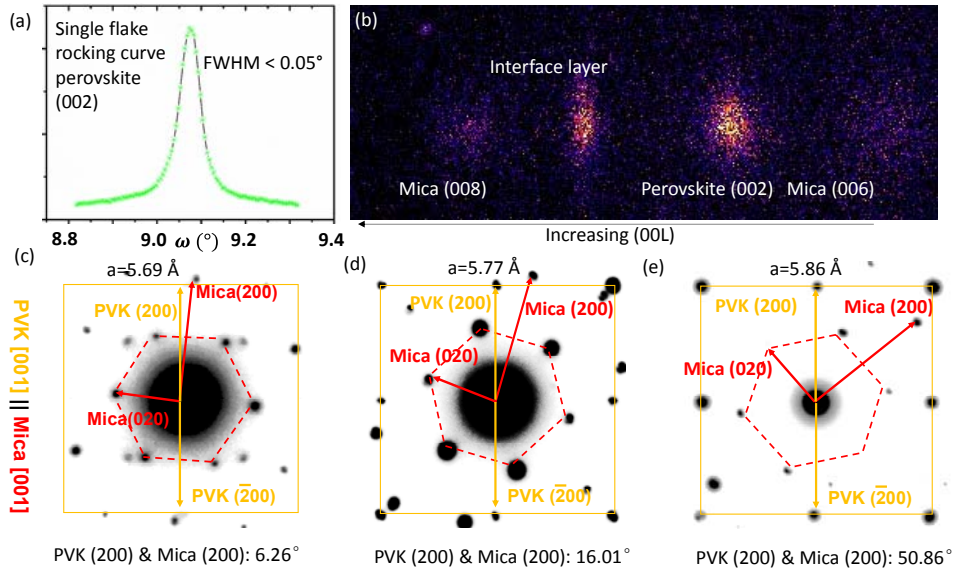
Fig. 2. Structural characterization of epitaxial halide perovskite on mica. (a) Synchrotron X-ray diffraction rocking curve of (002) peak from a single MAPbBr$_3$ flake. (b) Synchrotron X-ray diffraction 00L scan of halide perovskite on mica. Apart from the (006) and (008) diffraction from mica, and the (002) diffraction from perovskite, another diffraction pattern is also recorded that could come from an interfacial layer. (c-e) TEM planar view electron diffraction patterns of halide perovskite grown on mica substrate with (c) MAPbCl$_3$ and (d-e) CsPbBr$_3$. Two sets of diffraction spots belonging to the substrate (red) and film (orange) have been indexed. Halide perovskite with different lattice constants result in a different incommensurate epitaxial angle with the mica substrate. The angle dependence of lattice constant has been labeled.
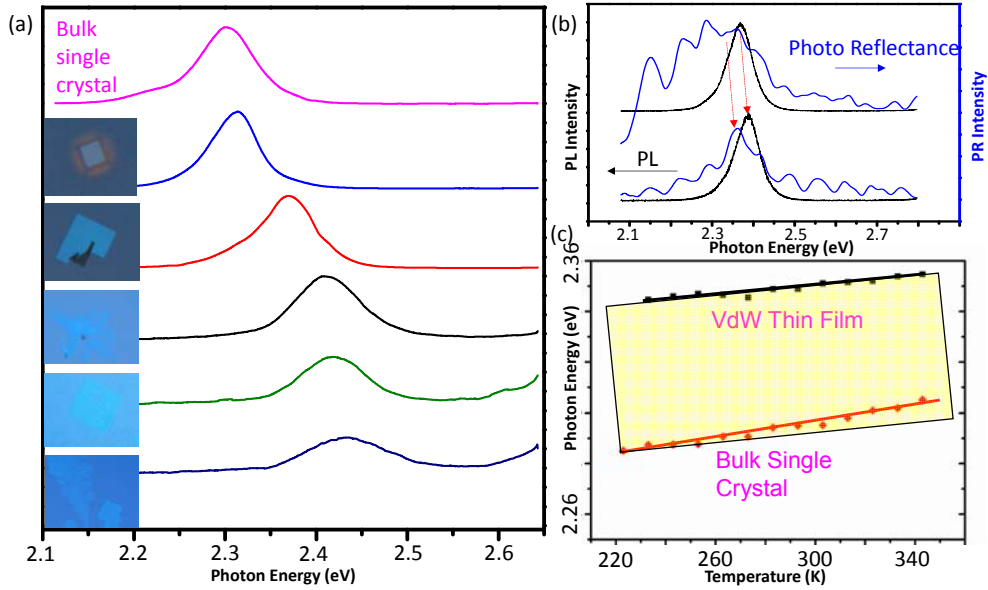
Fig. 3. Optical characterization of halide perovskite flakes on mica. (a) PL spectra of MAPbBr$_3$ flakes with different thicknesses. A significant blue shift of PL peaks with decreasing thickness is observed. The optical image to the left shows each flake where the spectrum is acquired. The color contrast of the optical image can be used to deduce the relative thickness of the flake. (b) PL spectra (black) and micro-PR spectra of the same CsPbBr$_3$ flakes. The two kinds of characterization show a consistent shift of peaks, indicating a difference in the band structure. (c) Temperature dependent PL spectra of vdW epitaxial thin film and bulk single crystal. A remarkable difference in the slopes can be observed. The vdW thin film follows more to the thermal expansion of the substrate when changing temperature.
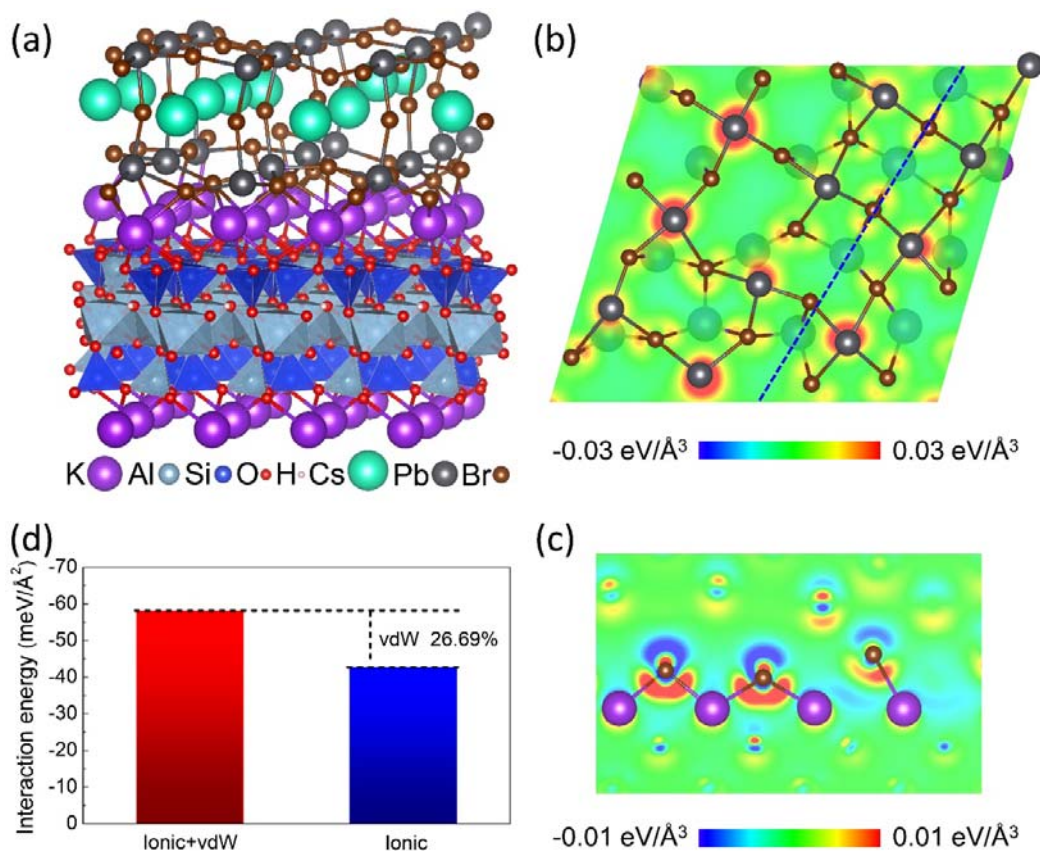
Fig. 4. DFT simulation of the interfacial interaction between epitaxial halide perovskite CsPbBr₃ and mica substrate. (a) Atomistic model of the relaxed supercell used in DFT calculations. The atoms have been labeled and drawn to its relative sizes. (b) The planar view of atomic stacking and charge transfer at the CsPbBr₃/mica interface. (c) Cross section noted as the blue dashed line in (b), and a significant charge transfer between the Potassium and Bromine atoms can be observed. (d) Calculation of the interaction energy at the interface that with and without vdW interaction. The vdW interaction takes a significant portion of the overall interaction energy, meaning a relative strong vdW force.

References

1.	H. Margenau, Van der Waals forces. *Reviews of Modern Physics* **11**, 1 (1939).
2.	Y. Zhang, Y.-W. Tan, H. L. Stormer, P. Kim, Experimental observation of the quantum Hall effect and Berry's phase in graphene. *nature* **438**, 201-204 (2005).
3.	K. S. Novoselov, A. K. Geim, S. Morozov, D. Jiang, M. Katsnelson, I. Grigorieva, S. Dubonos, Firsov, AA, Two-dimensional gas of massless Dirac fermions in graphene. *nature* **438**, 197-200 (2005).
4.	D. Pacile, J. Meyer, Ç. Girit, A. Zettl, The two-dimensional phase of boron nitride: few-atomic-layer sheets and suspended membranes. *Applied Physics Letters* **92**, 133107 (2008).
5.	G. Eda, H. Yamaguchi, D. Voiry, T. Fujita, M. Chen, M. Chhowalla, Photoluminescence from chemically exfoliated MoS2. *Nano letters* **11**, 5111-5116 (2011).
6.	H. Li, J. Wu, Z. Yin, H. Zhang, Preparation and applications of mechanically exfoliated single-layer and multilayer MoS2 and WSe2 nanosheets. *Accounts of chemical research* **47**, 1067-1075 (2014).
7.	A. Koma, Van der Waals epitaxy—a new epitaxial growth method for a highly lattice-mismatched system. *Thin Solid Films* **216**, 72-76 (1992).
8.	M. I. B. Utama, Q. Zhang, J. Zhang, Y. Yuan, F. J. Belarre, J. Arbiol, Q. Xiong, Recent developments and future directions in the growth of nanostructures by van der Waals epitaxy. *Nanoscale* **5**, 3570-3588 (2013).
9.	Y. Wang, Y. Shi, G. Xin, J. Lian, J. Shi, Two-dimensional van der Waals epitaxy kinetics in a three-dimensional perovskite halide. *Cryst. Growth Des* **15**, 4741-4749 (2015).
10.	J. Wu, C. Tan, Z. Tan, Y. Liu, J. Yin, W. Dang, M. Wang, H. Peng, Controlled Synthesis of High-Mobility Atomically Thin Bismuth Oxyselenide Crystals. *Nano Letters* **17**, 3021-3026 (2017).
11.	J. Wu, H. Yuan, M. Meng, C. Chen, Y. Sun, Z. Chen, W. Dang, C. Tan, Y. Liu, J. Yin, High electron mobility and quantum oscillations in non-encapsulated ultrathin semiconducting Bi2O2Se. *Nature Nanotechnology* **12**, 530-534 (2017).
12.	C. H. Lui, L. Liu, K. F. Mak, G. W. Flynn, T. F. Heinz, Ultraflat graphene. *Nature* **462**, 339-341 (2009).
13.	A. Rudenko, F. Keil, M. Katsnelson, A. Lichtenstein, Graphene adhesion on mica: Role of surface morphology. *Physical Review B* **83**, 045409 (2011).
14.	C. Jin, J. Kim, J. Suh, Z. Shi, B. Chen, X. Fan, M. Kam, K. Watanabe, T. Taniguchi, S. Tongay, Interlayer electron–phonon coupling in WSe 2/hBN heterostructures. *Nature Physics* **13**, 127 (2017).
15.	R. Viswanathan, J. Zasadzinski, D. Schwartz, in *PROCEEDINGS OF THE ANNUAL MEETING-ELECTRON MICROSCOPY SOCIETY OF AMERICA*. (JSTOR, 1993), pp. 514-514.
16.	C. Woods, L. Britnell, A. Eckmann, R. Ma, J. Lu, H. Guo, X. Lin, G. Yu, Y. Cao, R. Gorbachev, Commensurate-incommensurate transition in graphene on hexagonal boron nitride. *Nature physics* **10**, 451-456 (2014).
17.	Y. Wang, Y.-Y. Sun, S. Zhang, T.-M. Lu, J. Shi, Band gap engineering of a soft

inorganic compound PbI2 by incommensurate van der Waals epitaxy. *Applied Physics Letters* **108**, 013105 (2016).

18. G. H. Ahn, M. Amani, H. Rasool, D.-H. Lien, J. P. Mastandrea, J. W. Ager III, M. Dubey, D. C. Chrzan, A. M. Minor, A. Javey, Strain-engineered growth of two-dimensional materials. *Nature communications* **8**, 608 (2017).

19. N.-G. Park, Perovskite solar cells: an emerging photovoltaic technology. *Materials Today* **18**, 65-72 (2015).

20. M. D. McGehee, Perovskite solar cells: continuing to soar. *Nature materials* **13**, 845-846 (2014).

21. Q. Chen, N. De Marco, Y. M. Yang, T.-B. Song, C.-C. Chen, H. Zhao, Z. Hong, H. Zhou, Y. Yang, Under the spotlight: The organic–inorganic hybrid halide perovskite for optoelectronic applications. *Nano Today* **10**, 355-396 (2015).

22. Y. Wang, X. Sun, R. Shivanna, Y. Yang, Z. Chen, Y. Guo, G.-C. Wang, E. Wertz, F. Deschler, Z. Cai, Photon transport in one-dimensional incommensurately epitaxial CsPbX3 arrays. *Nano letters* **16**, 7974-7981 (2016).

23. Y. Rakita, S. R. Cohen, N. K. Kedem, G. Hodes, D. Cahen, Mechanical properties of APbX3 (A= Cs or CH3NH3; X= I or Br) perovskite single crystals. *MRS Communications* **5**, 623-629 (2015).

24. See Supplemental Material at [URL will be inserted by publisher] for more details on Materials and Methods, Characterizations Setups, AFM and Synchrotron Diffractions.

25. L. B. Freund, S. Suresh, *Thin film materials: stress, defect formation and surface evolution*. (Cambridge University Press, 2004).

26. W. K. Liu, M. B. Santos, *Thin films: heteroepitaxial systems*. (World Scientific, 1999), vol. 15.

27. A. Baskaran, P. Smereka, Mechanisms of stranski-krastanov growth. *J. Appl. Phys.* **111**, 044321 (2012).

28. I. Daruka, A.-L. Barabási, Dislocation-free island formation in heteroepitaxial growth: a study at equilibrium. *Physical Review Letters* **79**, 3708 (1997).

29. A. D. Novaco, J. P. McTague, Orientational epitaxy—the orientational ordering of incommensurate structures. *Physical Review Letters* **38**, 1286 (1977).

30. C. G. Shaw, S. Fain Jr, M. Chinn, Observation of orientational ordering of incommensurate argon monolayers on graphite. *Physical Review Letters* **41**, 955 (1978).

31. J. Liu, Y. Xue, Z. Wang, Z.-Q. Xu, C. Zheng, B. Weber, J. Song, Y. Wang, Y. Lu, Y. Zhang, Two-dimensional CH3NH3PbI3 perovskite: synthesis and optoelectronic application. (2016).

32. D. Li, G. Wang, H.-C. Cheng, C.-Y. Chen, H. Wu, Y. Liu, Y. Huang, X. Duan, Size-dependent phase transition in methylammonium lead iodide perovskite microplate crystals. *Nature communications* **7**, (2016).

33. E. Oksenberg, E. Sanders, R. Popovitz-Biro, L. Houben, E. Joselevich, Surface-Guided CsPbBr3 Perovskite Nanowires on Flat and Faceted Sapphire with Size-Dependent Photoluminescence and Fast Photoconductive Response. *Nano letters*, (2017).

34. Y. Fang, H. Wei, Q. Dong, J. Huang, Quantification of re-absorption and re-emission

processes to determine photon recycling efficiency in perovskite single crystals. *Nature Communications* **8**, (2017).

35. Y. Yamada, T. Yamada, L. Q. Phuong, N. Maruyama, H. Nishimura, A. Wakamiya, Y. Murata, Y. Kanemitsu, Dynamic optical properties of CH3NH3PbI3 single crystals as revealed by one-and two-photon excited photoluminescence measurements. *Journal of the American Chemical Society* **137**, 10456-10459 (2015).

36. J. S. Manser, P. V. Kamat, Band filling with free charge carriers in organometal halide perovskites. *Nature Photonics* **8**, 737-743 (2014).

37. Y. Wang, Z. Chen, F. Deschler, X. Sun, T.-M. Lu, E. A. Wertz, J.-M. Hu, J. Shi, Epitaxial Halide Perovskite Lateral Double Heterostructure. *ACS nano* **11**, 3355-3364 (2017).

38. Y. Yang, M. Yang, K. Zhu, J. C. Johnson, J. J. Berry, J. Van De Lagemaat, M. C. Beard, Large polarization-dependent exciton optical Stark effect in lead iodide perovskites. *Nature communications* **7**, 12613 (2016).

39. T. J. Jacobsson, L. J. Schwan, M. Ottosson, A. Hagfeldt, T. Edvinsson, Determination of thermal expansion coefficients and locating the temperature-induced phase transition in methylammonium lead perovskites using x-ray diffraction. *Inorganic chemistry* **54**, 10678-10685 (2015).

40. L. Goldstein, B. Post, Thermal expansion coefficients of ruby muscovite mica. *J. Appl. Phys.* **40**, 3056-3057 (1969).

41. G. Kresse, J. Furthmüller, Efficient iterative schemes for ab initio total-energy calculations using a plane-wave basis set. *Physical review B* **54**, 11169 (1996).

42. P. E. Blöchl, Projector augmented-wave method. *Physical review B* **50**, 17953 (1994).

43. J. Klimeš, D. R. Bowler, A. Michaelides, Chemical accuracy for the van der Waals density functional. *Journal of Physics: Condensed Matter* **22**, 022201 (2009).

44. J. Klimeš, D. R. Bowler, A. Michaelides, Van der Waals density functionals applied to solids. *Physical Review B* **83**, 195131 (2011).

45. T. Björkman, Testing several recent van der Waals density functionals for layered structures. *The Journal of chemical physics* **141**, 074708 (2014).

46. B. E. Deal, The oxidation of silicon in dry oxygen, wet oxygen, and steam. *Journal of the Electrochemical Society* **110**, 527-533 (1963).

47. A. Kozbial, Z. Li, C. Conaway, R. McGinley, S. Dhingra, V. Vahdat, F. Zhou, B. D'Urso, H. Liu, L. Li, Study on the surface energy of graphene by contact angle measurements. *Langmuir* **30**, 8598-8606 (2014).